CrystEngComm

ROYAL SOCIETY OF CHEMISTRY

PAPER

View Article Online
View Journal | View Issue

Cite this: *CrystEngComm*, 2020, **22**, 1875

Synthesis of a biocompatible nanoporous zeolitic imidazolate framework-8 in the presence of Gum Arabic inspired by the biomineralization process†

Seyedeh Fatemeh Khalilian,[a] Maryam Tohidi *[a] and Banafsheh Rastegari[b]

Received 3rd December 2019,
Accepted 13th January 2020

DOI: 10.1039/c9ce01915d

rsc.li/crystengcomm

Here, by inspiration from the natural biomineralization process, the one-pot synthesis of a zeolitic imidazolate framework-8 (ZIF-8, containing Zn^{2+} as a metal center and 2-methyl imidazole as a linker) was done in the presence of polysaccharide (Gum Arabic, GA), which enhanced its biocompatibility for application in the drug delivery systems. To the best of our knowledge, it is the first report on the synthesis of ZIF-8 in the presence of GA. The effect of some parameters such as the concentration of GA, the linker/metal molar ratio, and the water amount was investigated on the size, morphology, and crystallinity of the as-synthesized structures. The products were characterized *via* field emission scanning electron microscopy (FESEM), X-ray diffraction (XRD), Fourier transform infrared (FTIR) spectroscopy, Brunauer–Emmett–Teller (BET) surface area, thermogravimetric analysis (TGA), and UV-vis spectroscopic techniques. In addition, the standard 3-(4,5 dimethylthiazol-2-yl)-2,5-diphenyltetrazolium bromide (MTT) assay was performed on the human normal fibroblast cell line to compare the cytotoxicity of the ZIF-8 and ZIF-8–GA structures. The results showed the enhanced biocompatibility of ZIF-8–GA compared to ZIF-8 due to the presence of GA in the ZIF-8 framework.

Introduction

The biomineralization process is occurring when living organisms try to fabricate outer molecular architectures in order to provide a structural support to their soft tissues. By inspiration from the natural biomineralization process, this phenomenon can be used for the encapsulation of bioactive molecules such as polysaccharides, proteins, DNA, and enzymes within a protective exterior layer.[1]

Nanoporous metal–organic frameworks (MOFs) are provided by the inorganic and organic units linked together by strong bonds. They have demonstrated great potential for numerous applications such as in catalysis,[2–4] optics,[5] sensing,[6] gas storage,[7] and nanomedicine, including drug delivery,[8] and imaging.[9] However, the application of MOFs in nanomedicine has some disadvantages involving the degradation of the framework that can lead to the release of undesired components such as cations and organic ligands with toxic effects on the physiological media.[10,11] In order to prevent these unwanted effects, researchers suggested the use of BioMOFs, which were constructed by bioactive cations (such as Ca, Mg, Zn, and Fe) and *endo* (such as fumaric acid that was used for the synthesis of MIL-88A[12]) or *exo* (such as terephthalic acid that was used for the fabrication of MOF-5[13]) ligands.[14,15]

Recently, the synthesis of MOFs by the inspiration from the natural biomineralization process in the presence of biomacromolecules containing proteins, lipids, DNA, enzymes, polysaccharides as the crystallization and directing agents has been reported for the engineering of the novel type of BioMOFs.[1,4,16–19] In addition, some reports used cellulose-based materials, for instance plants,[20] cell nanofibers,[21] and cell nanocrystals[22] for the synthesis of MOFs and also creating biomolecule-MOF structures. Biomacromolecules quickly stimulate the fabrication of the more crystalline MOF shells by concentrating the building blocks of the framework on their surroundings.[23] These as-synthesized MOFs can be potentially applicable in the biological applications. The presence of biomolecules in the synthesis media can eliminate the usage of organic solvents, reduce the cytotoxicity of MOFs, and improve their applications in drug delivery systems.

Zeolitic imidazolate frameworks (ZIFs) are a kind of MOF that has been used in many studies due to its high surface area and exceptional chemical and thermal stability. In general, ZIFs are made by the coordination between M^{2+} cations and Imi (imidazolate) anions. Metal cations determined the name of ZIF, for example ZIF-8 was

[a] *Department of Nanochemical Engineering, Faculty of Advanced Technologies, Shiraz University, Shiraz, Iran. E-mail: matohidi@shirazu.ac.ir*
[b] *Diagnostic Laboratory Sciences and Technology Research Center, School of Paramedical Sciences, Shiraz University of Medical Sciences, Shiraz, Iran*

† Electronic supplementary information (ESI) available. See DOI: 10.1039/c9ce01915d

constructed by Zn^{2+} metal cations.[24] The homogenous phase of ZIF-8 crystals is a truncated rhombic dodecahedron.[25] In the biological applications, it shows the cytotoxicity effects at the concentration above 30 μg ml^{-1}.[26] There are some reports in the literature about the biocompatibility enhancement of ZIF-8 nanoparticles by using some coatings onto their surfaces such as hyaluronic acid (HA), polydopamine (PDA), and ZrO_2.[27–29] However, in these cases, the modification process was multi-steps or complicated involving several reagents.[27–29] Also, in some studies, ZIF-8 was used as a protective agent around biomacromolecules, such as dextran polysaccharide, bovine serum albumin (BSA), DNA, enzymes, and living cells.[1,16,30,31] As reported in the literature, the biomineralization process can overcome the problem of biocompatibility.[32] However, to the best of our knowledge, there is no investigation about increasing the biocompatibility of MOFs *via* the biomineralization process.

In this study, we used Gum Arabic (GA) polysaccharide for the first time as a biomacromolecule for the one-pot synthesis of ZIF-8–GA bioMOF in aqueous media after being inspired from the natural biomineralization process. GA is a kind of heterogeneous polysaccharide with a plant source (obtained from the acacia tree) that possesses several beneficial features such as biocompatibility, nontoxicity, and high water solubility. It is a branched and complex polysaccharide containing arabinose, rhamnose, galactose, and glucuronic acid residues.[33–35] The effects of some parameters such as the concentration of GA, linker/metal molar ratio, and water amount were investigated on the size, morphology, and crystallinity of the as-synthesized structures. The products were characterized *via* field emission scanning electron microscopy (FESEM), X-ray diffraction (XRD), Fourier transform infrared (FTIR) and UV-vis spectroscopy, Brunauer–Emmett–Teller (BET) surface area, and thermogravimetric analysis (TGA) techniques. Also, the standard 3-(4,5 dimethylthiazol-2-yl)-2,5-diphenyltetrazolium bromide (MTT) assay was performed on the fibroblast cell line (normal cell) for comparing the cytotoxicity of the ZIF-8 and ZIF-8–GA structures and investigating their biocompatibility.

Experimental

Chemicals

Zinc acetate dihydrate ($Zn(OAc)_2{\cdot}2H_2O$, 98%), 2-methyl imidazole (HmIm, 99%) and GA were purchased from MERCK. Phosphate buffer saline (PBS), Dulbecco's modified Eagle medium (DMEM) and the materials for the MTT assay were purchased from Sigma-Aldrich. All chemicals were used without any further purification. The water used in all the experiments was the distilled water. The human normal fibroblast cell lines were purchased from the Pasteur Institute of Iran.

Synthetic procedures

The synthesis of the ZIF-8 framework in the presence of GA in aqueous media was performed under various conditions: different concentrations of GA (2.0, 10.0, 15.0, and 20.0 mg ml^{-1}), molar ratios of linker/metal (4.0, 10.0, and 20.0), and amounts of water (2.5, 5.0, and 10.0 ml) were used for the synthesis. At the optimum condition, 6.0 ml of an aqueous solution of GA (150.0 mg) was provided. The solution was centrifuged in order to remove an excess amount of GA, and a uniform solution was obtained. Subsequently, the prepared aqueous solutions of zinc acetate dihydrate (43.9 mg, 1.0 ml) and HmIm (328.5 mg, 3.0 ml) were added simultaneously to the GA solution (total solution volume: 10.0 ml and linker/metal molar ratio: 20.0). Immediately the solution became opaque, and the crystals of ZIF-8 were formed. After one day, the reaction was completed, and the product was centrifuged and washed three times with water. The crystals of ZIF-8–GA were dried in a vacuum oven at 40 °C for one day. As a control, the synthesis of ZIF-8 was done in the absence of GA under the same synthesis condition for comparison.

Characterization techniques

FESEM images were recorded on a Hitachi S-4160 at an accelerating voltage of 20 kV. The SEM analysis was performed on TESKAN-Vega 3. The XRD patterns were recorded using a D8 ADVANCE type (BRUKER-Germany) with Cu Kα radiation (λ = 0.1542 nm). These patterns were taken in steps of 0.02°, with a sampling time of 1 s per step in the range of 2θ [5–50°]. The absorbance measurements were made using a Shimadzu 1601 PC UV-vis spectrophotometer. The FTIR spectra were recorded with tensor II (BRUKER-Germany). The TGA analysis was performed on a TGA/DSC 1-thermogravimetric analyzer that was made by Mettler-Toledo International Inc., under a nitrogen atmosphere from room temperature to 800 °C at the heating rate of 5 °C min^{-1}. The BET analysis was done by Micrometric (USA), ASAP 2020 instrument. The absorbance of the solution for the MTT assay was recorded using a plate reader Polar Star Omega, BMG LABTECH, Germany instrument.

MTT assay

Cytotoxicity was evaluated using the human normal fibroblast cell line. For this purpose, the cell line was sub-cultured in complete media, containing high glucose Dulbecco's modified Eagle medium (DMEM) supplemented with 10% heat-inactivated fetal bovine serum (FBS) in the presence of 1% penicillin/streptomycin at 37.0 °C under a humidified atmosphere of 5% CO_2. After reaching 90% of cell confluency, cells were trypsinized with 0.25% pre-warmed trypsin, followed by seeding 1.5×10^4 cells/well for normal skin fibroblast into 96 well plates overnight under the above condition. The next day, the medium was replaced by 100 μL of fresh culture medium containing 5.0, 10.0, 20.0, 30.0, 50.0, 75.0, and 100.0 μg ml^{-1} of ZIF-8 and ZIF-8–GA. After 24, 48, and 72 h of incubation, cells were washed two times with PBS and incubated in a fresh medium containing 0.5 mg ml^{-1} of the MTT solution. The plates were covered by an aluminium foil and incubated in an incubator under CO_2

pressure for 4 h. Thereafter, the culture medium was removed, and the formazan crystals were formed, to which 100 μl of solubilization solution (40.0% (v/v) DMF, 16.0% (w/v) SDS, pH = 4.7) was added. Finally, the absorbance of the solution was recorded at a wavelength of 570 nm *via* the plate reader instrument. The cell viability was determined using the following formula:

$$\text{Cell Viability}(\%) = \frac{\text{A Sample} - \text{A Blank}}{\text{A Negative Control} - \text{A Blank}} \times 100$$

Results and discussion

The synthesis of the ZIF-8 framework was done in the presence of GA under different synthesis conditions.

Investigation of the effect of the GA amount on the morphology of the ZIF-8–GA framework

For the investigation of the effect of different amounts of GA on the as-synthesized ZIF-8–GA, some concentrations were selected before and after the critical micelle concentration (CMC) of GA containing 2.0, 10.0, 15.0, and 20.0 mg ml^{-1} with a linker/metal molar ratio of 4.0 and a total aqueous volume of 10.0 ml (the reported CMC of GA is 0.25% (w/v)).[36] The SEM analysis was done for the characterization of the obtained products. Fig. 1 shows the SEM images of the as-synthesized products with different amounts of GA. It is clear that the multi-layered structures were obtained in the presence of different amounts of GA and linker/metal molar ratio of 4.0 (Fig. 1A–D). As reported in the literature, the homogenous phase of ZIF-8 crystals was truncated rhombic dodecahedron.[37] The multi-layered structures were the intermediate products that could convert to the truncated rhombic dodecahedron with some alterations in the synthetic conditions.[37] In this case, the selected amount of GA was 15.0 mg ml^{-1} due to the more uniformity of the obtained structures in this amount. The morphology of the product in this amount was bow-tie like containing multilayer nanosheets. For comparison, the ZIF-8 was synthesized without GA under similar synthesis condition. In this case, the leaf-like structure was obtained (Fig. 1E). The difference in the obtained morphologies of ZIF-8 and ZIF-8–GA (Fig. 1C and E) is clear. Thus, it shows a significant role of GA in the synthesis of ZIF-8 in aqueous media.

Investigation of the effect of the linker/metal molar ratio on the morphology and crystallinity of the ZIF-8–GA framework

For the investigation of the effect of the molar ratio of linker/metal on the morphology of the obtained products, different ratios containing 4.0, 10.0, and 20.0 were selected in the presence of 15.0 mg ml^{-1} GA with a total aqueous volume of 10.0 ml. The FESEM images of the different linker/metal molar ratios are shown in Fig. 2. Only at the linker/metal molar ratio of 20.0, the truncated rhombic dodecahedron morphology with an average size of 287 nm was obtained (linker/metal/water molar ratio was 20/1/2800) (Fig. 2C). The obtained ZIF8-GA had a very smaller and uniform size with respect to many reported studies in aqueous media in this molar ratio.[37] In one report, the ZIF-8 particles prepared from the $Zn(OAc)_2$ metal precursor had an average particle size of around 1.0 μm at the linker/metal/water molar ratio of 20/1/1280.[37] In other lower linker/metal molar ratios (4.0 and 10.0

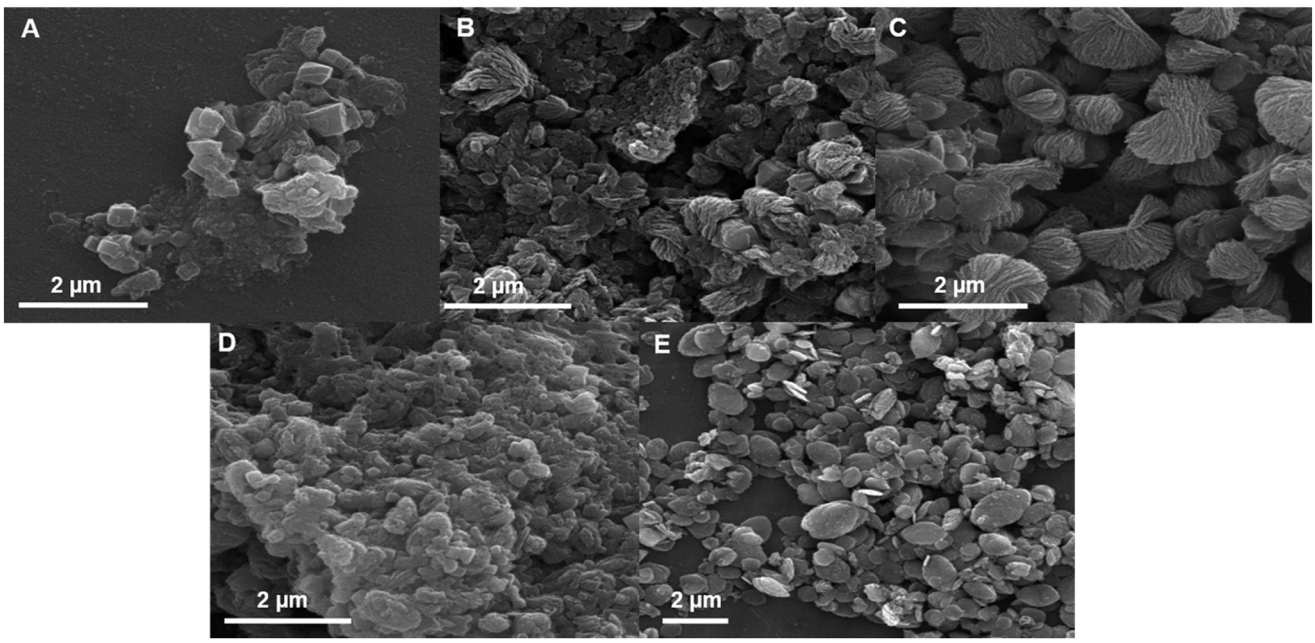

Fig. 1 SEM images of the synthesized ZIF-8–GA with A) 2.0, B) 10.0, C) 15.0 and D) 20.0 mg ml^{-1} of GA and (E) ZIF-8 without GA in a total volume of 10.0 ml and linker/metal molar ratio of 4.0.

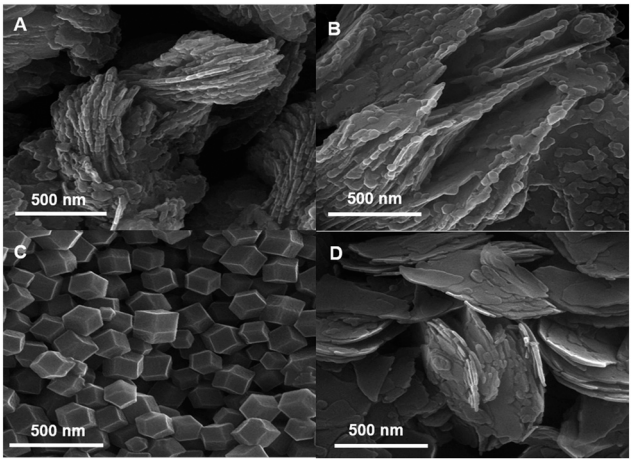

Fig. 2 FESEM images of the synthesized ZIF-8 with linker/metal molar ratios of A) 4.0, B) 10.0, and C) 20.0 in the presence of GA and D) 20.0 in the absence of GA at a total volume of 10.0 ml.

at the total aqueous volume of 10.0 ml), the morphology of the products was layered with an average thickness of 33 nm and 41.7 nm, respectively (Fig. 2A and B). For comparison, the synthesis of ZIF-8 at the linker/metal molar ratio of 20.0 was done in the absence of GA. In this case, layered sheets with an average thickness of 34 nm can be observed in the FESEM image (Fig. 2D). Thus, the results showed the importance of the presence of GA and also the amount of linker/metal molar ratio on the morphology of the obtained products.

Moreover, we noticed that the presence of GA triggered a rapid coordination reaction. The as-prepared solution in the presence of GA turned cloudy within 5 min containing spherical and layered structures (Fig. 3A and I), and after 20 min precipitates appeared with multilayered structures (Fig. 3B and I). After 1 h, the products with a truncated rhombic dodecahedron morphology were observed (Fig. 3C and I). The more uniform and complete dodecahedrons were obtained upon increasing the time up to 24 h (Fig. 3D, E, and I). In the absence of GA, the solution became cloudy after 1 h, and the precipitate appeared after 5 h containing multilayered structures (Fig. 3F, G, and J). The obtained morphology did not alter by increasing the time up to 24 h (Fig. 3H and J). This observation indicates that GA significantly accelerates the nucleation process of ZIF-8 crystals due to the coordination interactions between the hydroxyl groups of GA and Zn^{2+} ions. These interactions result in the enhancement of the local concentration of Zn^{2+} and aids the ZIF-8 nucleation around the GA and the formation of the truncated rhombic dodecahedron morphology.[38]

Also, the crystallinity of the as-synthesized ZIF-8–GA at different linker/metal molar ratios was studied *via* XRD analysis (Fig. 4). The best crystallinity was observed at a linker/metal molar ratio of 20.0 with a truncated rhombic dodecahedron

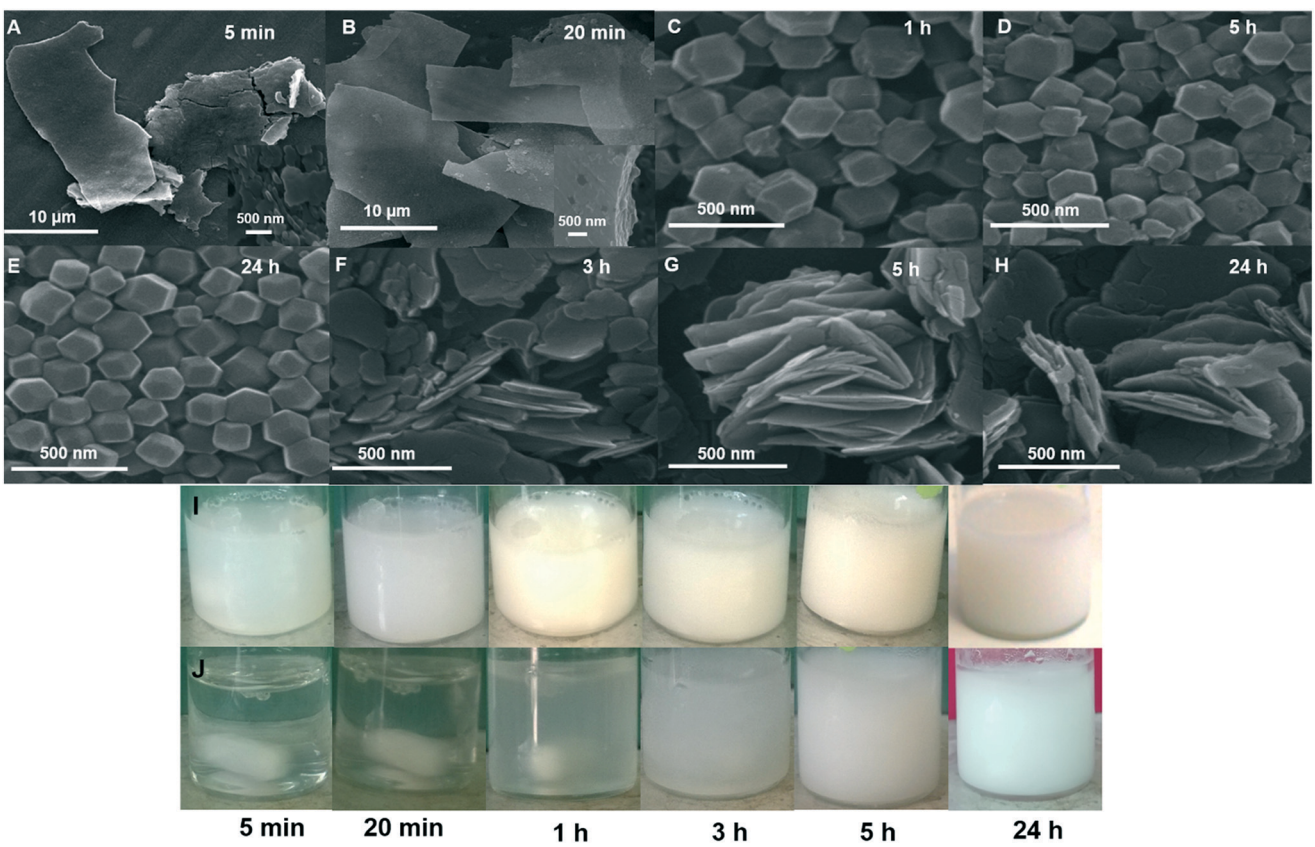

Fig. 3 SEM images and photographs of synthesis solution at linker metal molar ratio of 20.0/1.0/2800 as a function of time (A–E and I) in the presence and (F–H and J) absence of 15.0 mg ml^{-1} GA.

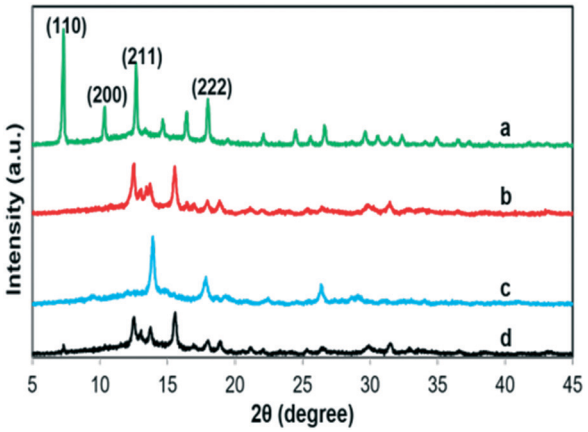

Fig. 4 The XRD patterns of ZIF-8–GA in linker/metal molar ratios of a) 20.0 b) 10.0 c) 4.0 in the presence of GA (15.0 mg ml^{-1} in a total volume of 10.0 ml) and d) 20.0 in the absence of GA.

morphology (Fig. 4a and 2C). The observed peaks at 2θ values of 7.29, 10.44, 12.83, and 18.10 match to the (110), (200), (211), and (222) index planes, respectively (Fig. 4a). They were the specific peaks of ZIF-8 that are reported in the literature, which confirmed the complete formation of the ZIF-8 framework, its stability, and minimum impact on its crystallinity in the presence of GA at a linker/metal molar ratio of 20.0.[37]

At other linker/metal molar ratios (4.0 and 10.0) with layered structures (Fig. 4b and c), some specific peaks of ZIF-8 such as dia(Zn) that correspond to the (110) index plane at 2θ values of 7.29, were not observed and also some unknown peaks appeared. As reported in the literature, these unknown peaks can be related to some other formed byproducts.[37] So in these molar ratios, the synthesis of the ZIF-8 framework was not complete, and the layered structures were obtained. Thus, the obtained results confirmed the significant role of the linker/metal molar ratios in the synthesis of uniform and homogeneous phases of ZIF-8–GA crystals in aqueous media.

Based on the previous report, the synthesis of a homogenous phase of ZIF-8 in the water solution needs a very high linker/metal molar ratio (such as 35.0 or 70.0 in a total volume of 10.0 ml) and also takes more time than the synthesis of ZIF-8 in the organic solvents.[37] Herein, the use of GA in the synthetic medium resulted in the reduction of required time and also the amount of linker/metal molar ratio (20.0 in a total volume of 10.0 ml) for the production of a homogenous phase of ZIF-8.

In addition, the XRD pattern of ZIF-8 in the absence of GA was analysed at a linker/metal molar ratio of 20.0 for comparison (Fig. 4d). As shown in Fig. 4d, the sharp peak of dia(Zn) was not observed. The result showed the key role of the presence of GA in the formation of a complete crystalline ZIF-8 framework in an aqueous solution.

Investigation of the effect of water amount on the morphology of the ZIF-8–GA framework

The effect of water amount was investigated on the morphology of the ZIF-8–GA framework. As reported in the literature, the linker/metal/water molar ratio can be very effective on the morphology and crystallinity of the obtained products.[37] In this study, the homogenous phase of ZIF-8–GA was obtained at a linker/metal/water molar ratio of 20/1/2800 (Fig. 2C). For the investigation of the amount of water, the lower total volume of water was examined for the linker/metal molar ratios that have layered structures in the case of a total aqueous volume of 10.0 ml. For this study, the amount of GA was fixed at 15.0 mg ml^{-1}, and the amount of linker/metal/water molar ratios were 4/1/1400, 10/1/1400, 4/1/700, and 10/1/700 in a total aqueous volumes of 5, 5, 2.5 and 2.5 ml, respectively. Fig. 5 shows the FESEM images of ZIF-8–GA in these conditions. The results showed that the amount of water can play a significant role in the formation of the homogenous phase of ZIF-8–GA. With the reduction in the water amount from 10.0 to 2.5 ml, the homogenous phase of ZIF-8–GA was obtained with an average size of 333.3 nm for a lower linker/metal/water molar ratio of 10/1/700 (Fig. 5D). In the case of a linker/metal/water molar ratio of 10/1/1400 in the total volume of water of 5.0 ml and linker/metal/water molar ratio of 4/1/1400 and 4/1/700 in the total volume of water of 5.0 and 2.5 ml, spherical and layered structures with an average size of 720 nm and thickness of 31.1 nm and 36.3 nm were obtained, respectively (Fig. 5A–C). It is worth noting that as reported in the literature, although spheres have been obtained instead of rhombic shapes in some synthesis conditions but had a typical ZIF-8 crystalline phase.[37] So, in this work, the crystalline phase of ZIF-8 in the presence of GA can be formed for the linker/metal/water molar ratios of 20/1/2800 and 10/1/700 with rhombic shapes and 10/1/1400 with a spherical shape (Fig. 2C, 5C and D). For comparison, ZIF-8 was synthesized in the linker/metal/water molar ratio of 10/1/700 in the absence of GA (Fig. 5E). Also, in this condition the decrease in the amount of water led to the formation of the homogenous phase of ZIF-8 crystals, but the crystals were not uniform and some large unusual structures appeared. The obtained result was in accordance with the literature.[37] Thus, it is clear that the presence of GA in this water amount has a key role in the formation of the homogenous phase of ZIF-8 crystals with smaller and uniform sizes and structures.

Confirming the presence of GA in the ZIF-8–GA framework

For confirming the presence of GA in the ZIF-8–GA framework, some analyses were done.

BET analysis

The BET adsorption analysis was performed to find out the surface area and porosity of ZIF-8–GA. The ZIF-8–GA BET isotherm is shown in Fig. 6. The isotherm showed a significant increase in the nitrogen adsorption at a low relative pressure, so the ZIF-8–GA isotherm is type-I (Langmuir isotherm) that confirmed the microporosity of ZIF-8–GA (Fig. 6). The BET surface area and pore volume of ZIF-8–GA were 1170.85 m^2 g^{-1} and 0.565 cm^3 g^{-1}, respectively. The obtained BET surface area and pore volume for ZIF-8–GA

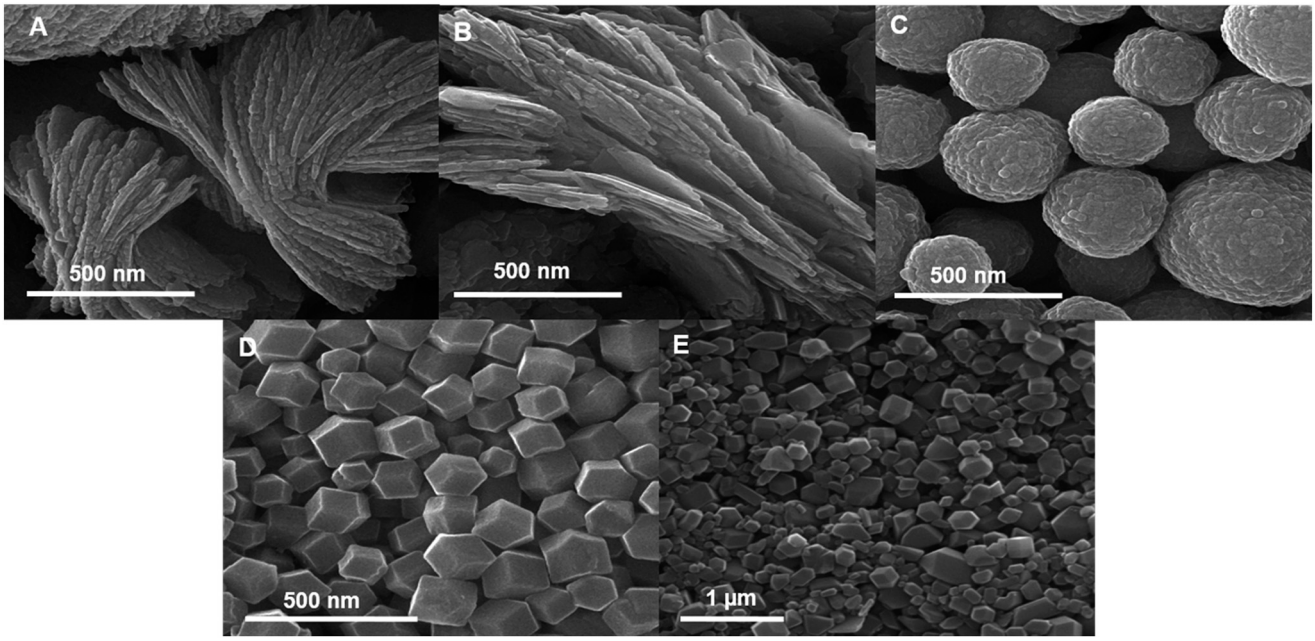

Fig. 5 FESEM images of ZIF-8 at different amount of linker/metal/water molar ratios A) 4/1/1400, B) 4/1/700, C) 10/1/1400, D) 10/1/700 in the presence of GA and E) 10/1/700 in the absence of GA.

were compared with the reported amount for ZIF-8 with the same morphology (1630–1700 $m^2\ g^{-1}$, 0.57 $cm^3 g^{-1}$).[37] The results indicated the reduction of these parameters for ZIF-8–GA with respect to ZIF-8 that confirmed the encapsulation of GA in the pores of ZIF-8–GA framework.

TGA analysis

The thermal stability of GA and ZIF-8–GA were investigated by TGA analysis. The results are shown in Fig. 7. GA starts to decompose at 265.52 °C and completed at 313.65 °C (Fig. 7a and S1A†). The thermal curve of ZIF-8–GA shows three zones of mass reduction (Fig. 7b). The first zone in the range of 166.61–202.71 °C corresponds to the solvent residue in the ZIF-8 pores that are reported in the literature.[39] The second zone matches the decomposition of GA that is present in the ZIF-8–GA structure in the range of 267.86–309.03 °C and the last zone between 558 and 752.33 °C relates to the decomposition of ZIF-8 framework (Fig. 7 and S1B†).[39] So, the results confirmed the encapsulation of GA in the ZIF-8–GA framework structure. TGA analysis was also applied for the quantitative investigation of the encapsulated GA from the mass loss in the temperature range of 268–309 °C (Fig. 7 and S1B†).[40] The encapsulation efficiency (EE) and loading capacity (LC) were then calculated using eqn (1) and (2), respectively. By considering the TGA data, the amounts of EE and LC were about 0.23% and 5.86%, respectively (Fig. S1B†).

$$\mathrm{EE}(\%) = \frac{\text{Total amount of loaded GA}}{\text{Initial amount of GA}} \times 100 \qquad (1)$$

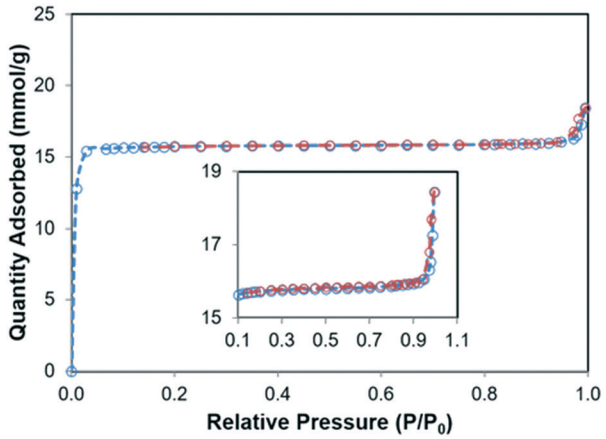

Fig. 6 Nitrogen adsorption–desorption isotherms of ZIF-8–GA.

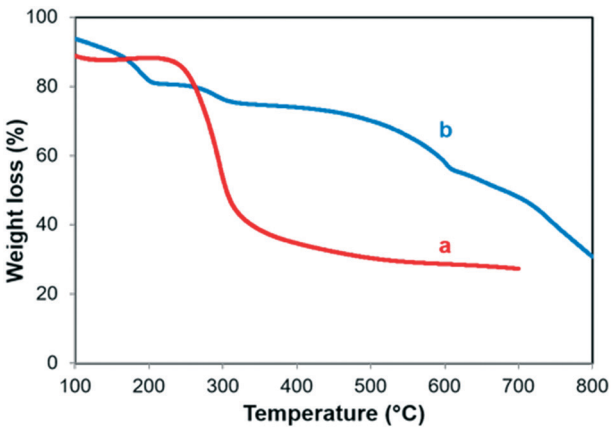

Fig. 7 TGA thermograms of a) GA and b) ZIF-8–GA.

$$\mathrm{LC}(\%) = \frac{\text{Total amount of loaded GA}}{\text{Weight of ZIF-8-GA after loss of solvent residue in TGA}} \times 100 \quad (2)$$

FT-IR analysis

The FT-IR analysis was done for ZIF-8, ZIF-8–GA, and GA (Fig. 8). As shown in Fig. 8a, the ZIF-8 framework had some specific peaks in the FT-IR analysis in accordance with the literature.[41] A sharp peak at 426 cm^{-1} was observed that corresponds to the Zn–N stretching vibration due to the connection of Zn^{2+} ions with the nitrogen atoms of the methylimidazole groups to form the imidazolate. The two peaks at 760 and 995 cm^{-1} were related to the C–H bending mode and C–N bending vibration, respectively. The peak at 694 cm^{-1} correlated to the ring out-of-plane bending vibration of the HmIm. The several spectral bands in the range of 1300–1460 cm^{-1} can be correlated to the entire ring stretching, while the band at 1149 cm^{-1} related to the aromatic C–N stretching mode. The peak at 1585 cm^{-1} could be due to the C–N stretching vibration.[42] In the case of ZIF-8–GA, the FT-IR spectrum verified the formation of ZIF-8 framework (Fig. 8b). For confirming the presence of GA in the structure, the FT-IR analysis was done for GA polysaccharide (Fig. 8c). The spectral bands falling between 3000–3600 cm^{-1} and 2800–3000 cm^{-1} corresponds to O–H (free or bonded) and C–H stretching modes, respectively (Fig. 8c). The peak at 1437.2 cm^{-1} may be due to the symmetrical stretching of carboxylic groups of uronic acid residues of gumpolysaccharides.[43,44] The peaks observed between 800 cm^{-1} and 1200 cm^{-1} represented C–O, C–C, and C–O–C stretching, and also C–O–H and C–H bending modes of the polymer backbone.[43] The comparison of the FT-IR analysis of GA and ZIF-8–GA showed that some specific peaks of GA containing broad peak between 800 and 1200 cm^{-1} and GA hydroxyl groups were shifted to the higher wavenumber in ZIF-8–GA structure which verified the encapsulation of GA in the ZIF-8–GA framework and its less flexibility (Fig. 8 and S2†).[1]

Also, as reported in the literature, the presence of many hydroxyl groups on the polysaccharides such as GA plays an important role in the biomimetic mineralization process due to the coordination interaction between the hydroxyl groups of GA and Zn^{2+} ions. This interaction results in the enhancement of the local concentration of Zn^{2+} and aids the ZIF-8 nucleation around the GA.[38]

UV-visible analysis

UV-visible spectroscopy was used in order to confirm the presence of GA in the ZIF-8–GA framework. Fig. 9 shows the UV-visible spectra of ZIF-8, ZIF-8–GA, and GA in the range of 200–800 nm. ZIF-8 and GA had one and two corresponding peaks at 211, 223, and 275 nm, respectively, in accordance with the literature (Fig. 9a and b).[45,46] The observed peaks for GA in the ZIF-8–GA framework (233 and 290 nm) had a red shift compared to free GA that confirmed the encapsulation of GA and its interrelated interactions in the framework (Fig. 9c).

Effect of GA on the dispersion of ZIF-8 in aqueous medium

GA has many hydroxyl, amino, and carboxyl groups that can affect the dispersion of ZIF-8–GA in water.[47] For the investigation of the effect of the encapsulation of GA in the ZIF-8 framework, a specific amount of ZIF-8 and ZIF-8–GA were dispersed in 10.0 ml water. As shown in Fig. 10, the presence of GA in the ZIF-8–GA structure leads to the more dispersion ability of ZIF-8–GA compared to ZIF-8 in water that can be very useful in biological and medical applications.[48]

The mechanism of ZIF-8 synthesis in aqueous media

Some studies described the mechanism of synthesis of ZIF-8 in the aqueous media in a five-step process

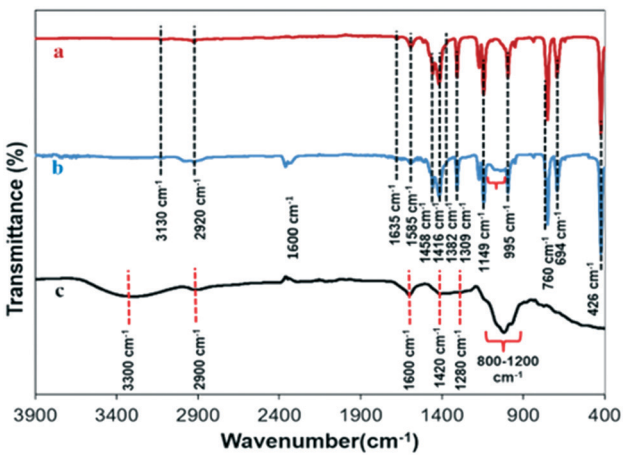

Fig. 8 FTIR analysis of a) ZIF-8, b) ZIF-8–GA, and c) GA.

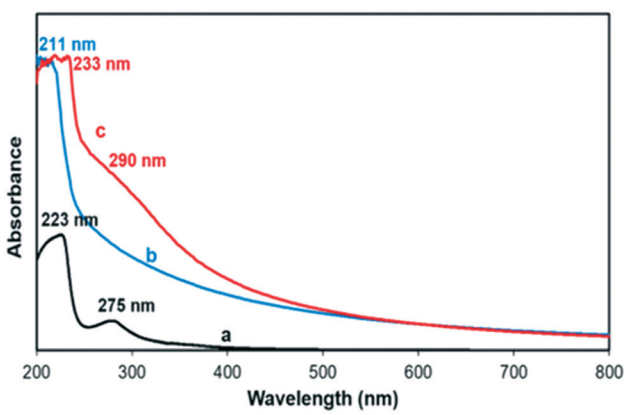

Fig. 9 UV-vis spectra of a) GA, b) ZIF-8, and c) ZIF-8–GA.

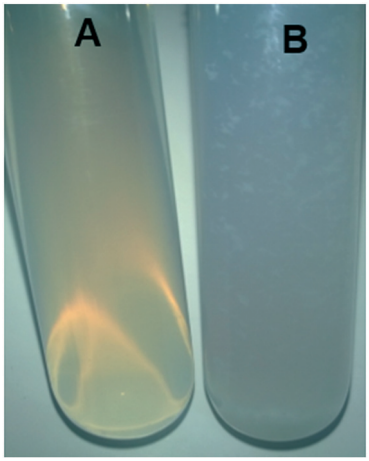

Fig. 10 Picture of dispersion of A) ZIF-8–GA and B) ZIF-8 in water.

containing:[37] 1. nucleation process that forms tiny crystals; 2. formation of 2D layered structures as a transient crystalline phase of ZIF-8; 3. random attachment of 2D layered units for the formation of multi-layered structures; 4. breaking down of stacked layers to smaller crystals in the presence of an excess of HmIm for the formation of ZIF-8 crystals; and 5. the growth of the metastable ZIF-8 nanocrystals *via* the Ostwald ripening process for the production of truncated rhomboid dodecahedron shape. As shown in Fig. 3A and B, the spherical and layered intermediate structures were observed at initial times. The truncated rhomboid dodecahedron morphology was obtained at longer times (Fig. 3C and D). The obtained results confirmed that the mechanism of the growth of ZIF-8–GA is similar to the ZIF-8 that is mentioned in the literature.[37]

Cytotoxicity studies

The biocompatibility of ZIF-8–GA was investigated by MTT assay on the human normal fibroblast cell line. Fig. 11 shows the cell viability percentage *versus* ZIF-8–GA and ZIF-8 concentrations (μg ml^{-1}) at various times (24, 48, and 72 h). The obtained results showed that ZIF-8 has significant cytotoxicity at concentrations above 30 μg ml^{-1} in a time-dependent manner (Fig. 11). Some reported studies also confirmed the cytotoxicity of ZIF-8 at concentrations above 30 μg ml^{-1} by increasing the ROS amount that results in DNA damage and cell death.[26] So, the used concentration of ZIF-8 is very limited for biological and medical applications.[26] In comparison, the ZIF-8–GA had more cell viability percent above 30 μg ml^{-1} concentrations, even at 75 μg ml^{-1} concentration after 72 h (Fig. 11C). The results showed that the presence of the negligible amount of GA (0.3381 mg) in the ZIF-8 (5.3513 mg) framework plays a significant role in the biocompatibility of the ZIF-8 framework (Fig. S1B†). As reported in the literature, the ROS mainly causes systematic bimolecular damages to the

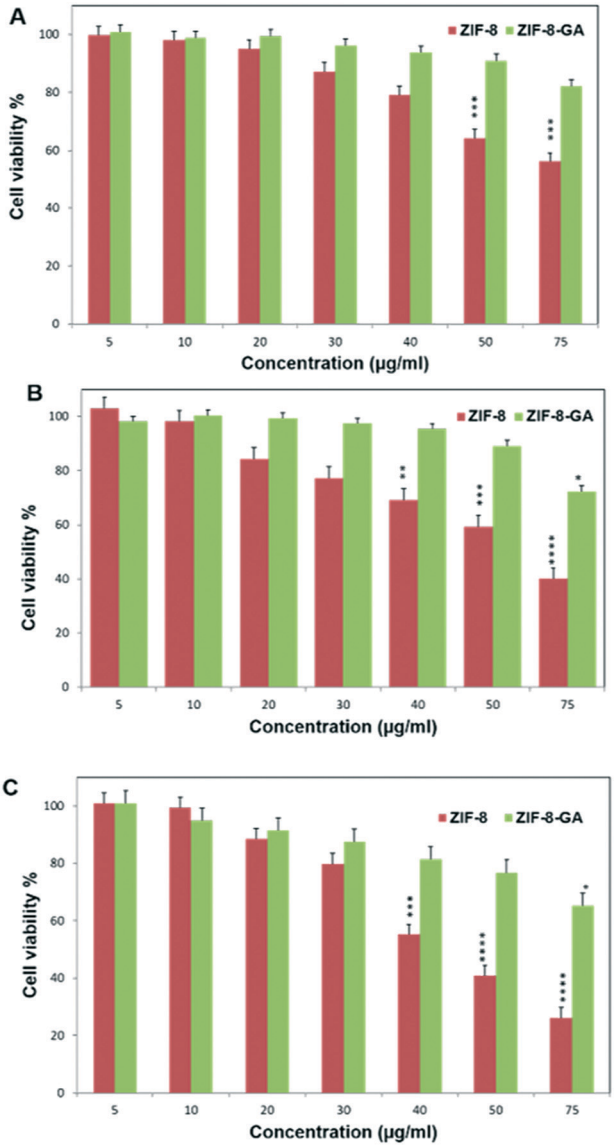

Fig. 11 MTT assay on normal skin fibroblast cell line in various time A) 24 h, B) 48 h, and C) 72 h.

nucleic acids, protein, carbohydrates, and lipids.[49] The increased biocompatibility of GA might be due to its antioxidant properties by chelating chemicals that can generate ROS such as Zn^{2+} not only from the body fluid, but also from hepatic and renal cells, which are mainly responsible for detoxification in animal models.[50,51] Moreover, the colloidal stability of the synthesized ZIF-8–GA framework is improved due to the highly branched polysaccharide structural nature (a large amount of hydroxyl, amino, and carboxyl groups) of GA which causes steric repulsion between nanoparticles.[35,47] In other point of view, galactose of GA can lead to enhanced targeting and uptake of drug carriers to lectin receptor containing cells such as hepatocyte, breast, and lung cancerous cells.[52] Therefore, this biocompatible ZIF-8–GA framework can be a good candidate for application as a drug delivery carrier

compared to ZIF-8 that has a magnificent potential in drug delivery but possesses some disadvantages like cytotoxicity.[26]

Conclusion

In this study, we mentioned a new strategy for the synthesis of ZIF-8 in aqueous media inspired by the biomineralization process. We used GA as a polysaccharide in order to synthesize ZIF-8–GA frameworks. All the characteristic analysis confirmed the effective synthesis of ZIF-8–GA structures with truncated rhomboid dodecahedron shape in aqueous media at optimum condition and the encapsulation of GA in the framework. The presence of GA not only reduced the amount of linker/metal ratio but also reduced the synthesis time. The obtained structures were smaller, uniform, and water-dispersible compared to many reported works. The MTT assay showed less toxicity of the ZIF-8–GA compared to ZIF-8. So, it's a very convenient way for the synthesis of biocompatible, less toxic, and water-dispersible ZIF-8 framework that can open a new way for the use of this structure in the biomedicine and drug delivery systems.

Conflicts of interest

There are no conflicts to declare.

Acknowledgements

This research was supported by Shiraz University and Iran Ministry of Science and Technology. The authors wish to thank all who assisted in conducting this work.

References

1 K. Liang, R. Wang, M. Boutter, C. M. Doherty, X. Mulet and J. J. Richardson, *Chem. Commun.*, 2017, **53**, 1249–1252.
2 L. Ma, J. M. Falkowski, C. Abney and W. Lin, *Nat. Chem.*, 2010, **2**, 838.
3 J. Liu, L. Chen, H. Cui, J. Zhang, L. Zhang and C.-Y. Su, *Chem. Soc. Rev.*, 2014, **43**, 6011–6061.
4 F.-K. Shieh, S.-C. Wang, C.-I. Yen, C.-C. Wu, S. Dutta, L.-Y. Chou, J. V. Morabito, P. Hu, M.-H. Hsu and K. C.-W. Wu, *J. Am. Chem. Soc.*, 2015, **137**, 4276–4279.
5 L. Mingabudinova, V. Vinogradov, V. Milichko, E. Hey-Hawkins and A. Vinogradov, *Chem. Soc. Rev.*, 2016, **45**, 5408–5431.
6 Z. Hu, B. J. Deibert and J. Li, *Chem. Soc. Rev.*, 2014, **43**, 5815–5840.
7 K. Sumida, D. L. Rogow, J. A. Mason, T. M. McDonald, E. D. Bloch, Z. R. Herm, T.-H. Bae and J. R. Long, *Chem. Rev.*, 2011, **112**, 724–781.
8 J. Bi, Y. Lu, Y. Dong and P. Gao, *J. Nanomater.*, 2018, **2018**, 1357812.
9 K. M. Taylor, W. J. Rieter and W. Lin, *J. Am. Chem. Soc.*, 2008, **130**, 14358–14359.
10 P. Horcajada, R. Gref, T. Baati, P. K. Allan, G. Maurin, P. Couvreur, G. Ferey, R. E. Morris and C. Serre, *Chem. Rev.*, 2011, **112**, 1232–1268.
11 A. C. McKinlay, R. E. Morris, P. Horcajada, G. Férey, R. Gref, P. Couvreur and C. Serre, *Angew. Chem., Int. Ed.*, 2010, **49**, 6260–6266.
12 C. Serre, F. Millange, S. Surblé and G. Férey, *Angew. Chem., Int. Ed.*, 2004, **43**, 6285–6289.
13 H. Li, M. Eddaoudi, M. O'Keeffe and O. M. Yaghi, *Nature*, 1999, **402**, 276.
14 I. Imaz, M. Rubio-Martínez, J. An, I. Sole-Font, N. L. Rosi and D. Maspoch, *Chem. Commun.*, 2011, **47**, 7287–7302.
15 R. S. Forgan, *Encyclopedia of Inorganic and Bioinorganic Chemistry*, 2011, pp. 1–13.
16 K. Liang, R. Ricco, C. M. Doherty, M. J. Styles, S. Bell, N. Kirby, S. Mudie, D. Haylock, A. J. Hill and C. J. Doonan, *Nat. Commun.*, 2015, **6**, 7240.
17 D. Feng, T.-F. Liu, J. Su, M. Bosch, Z. Wei, W. Wan, D. Yuan, Y.-P. Chen, X. Wang and K. Wang, *Nat. Commun.*, 2015, **6**, 5979.
18 X. Zhong, H. Xia, W. Huang, Z. Li and Y. Jiang, *Chem. Eng. J.*, 2020, **381**, 122758.
19 L. Qi, Z. Luo and X. Lu, *ACS Sustainable Chem. Eng.*, 2019, **7**, 7127–7139.
20 J. J. Richardson and K. Liang, *Small*, 2018, **14**, 1702958.
21 L. Zhu, L. Zong, X. Wu, M. Li, H. Wang, J. You and C. Li, *ACS Nano*, 2018, **12**, 4462–4468.
22 J. J. Richardson, B. L. Tardy, J. Guo, K. Liang, O. J. Rojas and H. Ejima, *ACS Sustainable Chem. Eng.*, 2019, **7**, 6287–6294.
23 J. Cravillon, C. A. Schröder, R. Nayuk, J. Gummel, K. Huber and M. Wiebcke, *Angew. Chem., Int. Ed.*, 2011, **50**, 8067–8071.
24 Y. V. Kaneti, S. Dutta, M. S. Hossain, M. J. Shiddiky, K. L. Tung, F. K. Shieh, C. K. Tsung, K. C. W. Wu and Y. Yamauchi, *Adv. Mater.*, 2017, **29**, 1700213.
25 S. R. Venna, J. B. Jasinski and M. A. Carreon, *J. Am. Chem. Soc.*, 2010, **132**, 18030–18033.
26 M. Hoop, C. F. Walde, R. Riccò, F. Mushtaq, A. Terzopoulou, X.-Z. Chen, A. J. deMello, C. J. Doonan, P. Falcaro and B. J. Nelson, *Appl. Mater. Today*, 2018, **11**, 13–21.
27 Y. Li, Y. Zheng, X. Lai, Y. Chu and Y. Chen, *RSC Adv.*, 2018, **8**, 23623–23628.
28 Q. Wu, M. Niu, X. Chen, L. Tan, C. Fu, X. Ren, J. Ren, L. Li, K. Xu and H. Zhong, *Biomaterials*, 2018, **162**, 132–143.
29 L. Su, Q. Wu, L. Tan, Z. Huang, C. Fu, X. Ren, N. Xia, Z. Chen, X. Ma and X. Lan, *ACS Appl. Mater. Interfaces*, 2019, **11**, 10520–10531.
30 F. Lyu, Y. Zhang, R. N. Zare, J. Ge and Z. Liu, *Nano Lett.*, 2014, **14**, 5761–5765.
31 K. Liang, J. J. Richardson, J. Cui, F. Caruso, C. J. Doonan and P. Falcaro, *Adv. Mater.*, 2016, **28**, 7910–7914.
32 Y. Chen, Y. Feng, J. G. Deveaux, M. A. Masoud, F. S. Chandra, H. Chen, D. Zhang and L. Feng, *Minerals*, 2019, **9**, 68.
33 S. Patel and A. Goyal, *Int. J. Food Prop.*, 2015, **18**, 986–998.
34 D. Verbeken, S. Dierckx and K. Dewettinck, *Appl. Microbiol. Biotechnol.*, 2003, **63**, 10–21.

35 V. Kattumuri, K. Katti, S. Bhaskaran, E. J. Boote, S. W. Casteel, G. M. Fent, D. J. Robertson, M. Chandrasekhar, R. Kannan and K. V. Katti, *Small*, 2007, **3**, 333–341.
36 A. Grein, B. C. da Silva, C. F. Wendel, C. A. Tischer, M. R. Sierakowski, A. B. D. Moura, M. Iacomini, P. A. Gorin, F. F. Simas-Tosin and I. C. Riegel-Vidotti, *Carbohydr. Polym.*, 2013, **92**, 312–320.
37 M. Jian, B. Liu, R. Liu, J. Qu, H. Wang and X. Zhang, *RSC Adv.*, 2015, **5**, 48433–48441.
38 L. Yang, Y. Su, Y. Xu, S. Zhang, J. Wu and K. Zhao, *J. Inorg. Biochem.*, 2004, **98**, 1251–1260.
39 T. Tian, J. Velazquez-Garcia, T. D. Bennett and D. Fairen-Jimenez, *J. Mater. Chem. A*, 2015, **3**, 2999–3005.
40 S. F. Hosseini, M. Zandi, M. Rezaei and F. Farahmandghavi, *Carbohydr. Polym.*, 2013, **95**, 50–56.
41 Y. Zhang, Y. Jia and L. A. Hou, *RSC Adv.*, 2018, **8**, 31471–31477.
42 Y. Hu, H. Kazemian, S. Rohani, Y. Huang and Y. Song, *Chem. Commun.*, 2011, **47**, 12694–12696.
43 M. Bashir and S. Haripriya, *Int. J. Biol. Macromol.*, 2016, **93**, 476–482.
44 H. Espinosa-Andrews, O. Sandoval-Castilla, H. Vázquez-Torres, E. J. Vernon-Carter and C. Lobato-Calleros, *Carbohydr. Polym.*, 2010, **79**, 541–546.
45 H. Adam, M. A. Siddig, A. A. Siddig and N. A. Eltahir, *Sudan Medical Monitor*, 2013, **8**, 174.
46 H. Kaur, G. C. Mohanta, V. Gupta, D. Kukkar and S. Tyagi, *J. Drug Delivery Sci. Technol.*, 2017, **41**, 106–112.
47 H. R. de Barros, M. B. Cardoso, C. C. de Oliveira, C. R. C. Franco, D. de Lima Bellan, M. Vidotti and I. C. Riegel-Vidotti, *RSC Adv.*, 2018, **8**, 40596.
48 H. R. de Barros, M. B. Cardoso, C. C. de Oliveira, C. R. C. Franco, D. de Lima Belan, M. Vidotti and I. C. Riegel-Vidotti, *RSC Adv.*, 2016, **6**, 9411–9420.
49 J. Lykkesfeldt and O. Svendsen, *Vet. J.*, 2007, **173**, 502–511.
50 N. O. Ayaz, K. S. Ramadan, H. E. Farid and H. S. Alnahdi, *Indian J. Anim. Res.*, 2017, **51**, 303–309.
51 W. Nasif, M. Lotfy and M. Mahmoud, *Riv. Eur. Sci. Med. Farmacol.*, 2011, **15**, 285–292.
52 Y. Ma, H. Chen, S. Su, T. Wang, C. Zhang, G. Fida, S. Cui, J. Zhao and Y. Gu, *J. Cancer*, 2015, **6**, 658.